Microsyst Technol (2010) 16:461–476
DOI 10.1007/s00542-009-0942-y

TECHNICAL PAPER

Performance optimization and mechanical modeling of uniaxial piezoresistive microaccelerometers

Angel R. Cortés-Pérez · Agustin Leobardo Herrera-May · Luz A. Aguilera-Cortés · Max A. González-Palacios · Miguel Torres-Cisneros

Received: 23 July 2009 / Accepted: 21 October 2009 / Published online: 17 November 2009

Abstract The acceleration measurements in automotive, navigation, biomedical and consumer applications demand high-performance microaccelerometers. This paper presents an optimization model to maximize the bandwidth of uniaxial piezoresistive microaccelerometers based on cantilever-type beams. The proposed model provides a high sensitivity as well as normal stress levels lower than the material rupture stress of these microaccelerometers. This model uses the Rayleigh method to determine the objective function of the bandwidth and the maximum-normal-stress failure theory to obtain a stress constraint that guarantees safe operation for the microaccelerometer structure. The Box-Complex optimization method is used to solve the optimization model due to its easy programming algorithm. Finite element models (FE) are developed to determine the mechanical behavior of the optimized piezoresistive microaccelerometers. The results of the FE models agree well with those of the optimization model. The optimization model can be easily used by designers to find the optimum geometrical dimensions of piezoresistive microaccelerometers to maximize their performance.

A. R. Cortés-Pérez · A. L. Herrera-May (✉) · L. A. Aguilera-Cortés · M. A. González-Palacios · M. Torres-Cisneros
Depto. Ingeniería Mecánica, Campus Irapuato-Salamanca, Universidad de Guanajuato, Carretera Salamanca-Valle de Santiago km 3.5+1.8 km, Salamanca, Guanajuato, Mexico
e-mail: leherrera@uv.mx

L. A. Aguilera-Cortés
e-mail: aguilera@salamanca.ugto.mx

A. L. Herrera-May
Centro de Investigación en Micro y Nanotecnología, Universidad Veracruzana, 94292 Boca del Río, Veracruz, Mexico

1 Introduction

Bulk and surface micromachining techniques have allowed the development of efficient sensors able to measure physical parameters such as acceleration (Herrera-May et al. 2008), magnetic field (Herrera-May et al. 2009a), and pressure (Herrera-May et al. 2009b). This has been stimulated by the advantages offered by micromachining techniques, including: miniaturization, low power consumption, high sensitivity, and low sensor price. Among these devices, microaccelerometers have obtained great success commercially mainly in the automotive industry, where they are used to activate safety systems, for example in air bags, vehicle stability systems, and electronic suspensions (Yazdi et al. 1998). In addition, other applications demanding high-performance microaccelerometers include navigation, biomedical activity monitoring, seismology, and consumer applications such as headsets for virtual reality and computer peripherals (Beeby et al. 2004; Fedder et al. 2005). Two main requirements for these microaccelerometers include high sensitivity and large bandwidth. Thus, an ideally designed microaccelerometer should have optimum performance to achieve these requirements. Unfortunately, the requirements conflict each other, so if the sensitivity is increased then the bandwidth is decreased and vice versa (Roylance and Angell 1979). Therefore, designers have an important challenge to determine optimum values of the sensitivity and bandwidth for each particular application. Seidel and Csepregi (1984) reported a design optimization procedure to maximize one of the requirements with a specific value for the other. In addition, the performance optimization of the accelerometers must guarantee safe operation (i.e., the stress caused by the accelerations should be less than the material rupture stress of the microaccelerometer).

During the last three decades various microaccelerometers have been investigated based on piezoresistive (Amarasinghe et al. 2007; Sankar et al. 2009), capacitance (Chae et al. 2005), piezoelectric (Hindrichsen et al. 2009), thermal (Dauderstädt et al. 1998), tunneling (Liu and Kenny 2001), and optical (Lee and Cho 2004) sensing principles. Each approach has its own inherent advantages and drawbacks. For example, piezoelectric microaccelerometers have a fast response, minimum power consumption, and good linearity, but do not respond to constant acceleration (Zhu et al. 2004). Thermal microaccelerometers do not need a solid proof mass and are based on thermal convection, although, they have offset variations for long term operation conditions caused by changes in the environment temperature (Kaltsas et al. 2006). Tunneling microaccelerometers present a high sensitivity, but they require a complex fabrication process and have stability problems (Liu et al. 1998). Novel designs include optical microaccelerometers that have immunity to electromagnetic interference (EMI) and reduce electronic circuitry and total weight; though, they present intrinsic losses due to structural imperfections and require difficult fabrication processes (Llobera et al. 2007). Capacitive microaccelerometers have a little dependence on the temperature, but they have parasitic capacitances of the connecting leads that complicate the measurements of the signal; in addition, they require complicated electronics and the narrow air gap over a relatively large area increases the damping (Zou et al. 2008). Piezoresistive microaccelerometers are fabricated using an easy and mature process, require simple readout circuits, have low cost and high sensitivity, but they suffer from thermal influences that can be controlled with careful packaging, trimming, and compensation circuits (Partridge et al. 2000; Huang et al. 2005). Piezoresistive microaccelerometers are an important alternative for use in conventional and new applications of acceleration measurements.

Although the research and fabrication of piezoresistive microaccelerometers have been very extensive, few studies about of their performance optimization have been realized. Seidel and Csepregi (1984) reported a design optimization procedure of a piezoresistive microaccelerometer to maximize its sensitivity while its bandwidth maintained a specific value, but without considering the stress caused by the accelerations. Joshi et al. (2005) proposed a technique for optimizing performance of a cantilever-type microaccelerometer based on finite element method (FEM) models through Coventoreware MEMSCAD software; however, this technique analyzes only the bandwidth variation and stresses caused by the changes in the dimensions of the cantilever. In addition, this technique requires much computation time to evaluate the performance of the FEM models. Kovács and Vízváry (2001) reported analytical models to estimate the bandwidth and sensitivity of piezoresistive microaccelerometers due to the change of geometrical parameters. However, Kovács and Vízváry (2001) do not developed optimization models to evaluate the optimum performance of the microaccelerometer and do not considered stress effect on the structure. Coultate et al. (2008) reported an optimum and robust design on a capacitive microaccelerometer using the genetic algorithm technique. Although, this technique is complicated and it is only used to maximize the full-scale range (FSR). These models have not been able to predict the optimal performance of a piezoresistive microaccelerometer. Nor is the method capable of determining the optimum dimensions of the structure to achieve a high sensitivity and high bandwidth. In addition, they neglect the structural stress generated by the accelerations. We propose an optimization model to find the optimum performance of piezoresitive microaccelerometers based on cantilever-type beams, which consider the maximum-normal-stress failure theory to guarantee safe operation of the microaccelerometer structure. This model finds the optimum geometrical dimensions of the cantilever-type microaccelerometers to achieve a maximum bandwidth and a high sensitivity. The model is solved using an algorithm based on the Box-Complex method, which is very easy to use. In addition, we utilized FEM models with ANSYS software to model the mechanical behavior (i.e., resonant frequencies and stress of the microaccelerometer structure) of the optimum microaccelerometer. Also, these models can be modified and adapted to other piezoresistive microaccelerometers that use other cantilever-type structures (e.g., double clamped cantilever). The Rayleigh method is used to determine the objective function (bandwidth of the microaccelerometer) of the optimization model. This model can be easily used by designers to determine the optimum dimensions of piezoresistive microaccelerometers which are based on cantilever-type structures. The proposed optimization model is adapted to a piezoresistive microaccelerometer developed by Plaza et al. (2002).

Following the introduction, the paper is organized as follows. Section 2 presents the description of the bandwidth, sensitivity and stress models of the piezoresistive microaccelerometer based on cantilever-type beams. Section 3 shows the variations of the bandwidth, sensitivity, and maximum normal stress of the piezoresistive microaccelerometer as a function of its geometrical parameters. Section 4 describes the proposed optimization model and Section 5 reports the results and discusses the results of the optimization model and the FE models. The

paper ends with the concluding discussion and a proposal for further work.

2 Description of the device models

A description of the bandwidth, sensitivity and stress models of a piezoresistive microaccelerometer is necessary to find its optimum performance for a specific application. These models are applied to the structural configuration of a piezoresistive microaccelerometer fabricated by Plaza et al. (2002). The models find the required geometrical dimensions of the microaccelerometer for an optimum bandwidth, a high sensitivity and a stress level less than the material rupture stress of its structure.

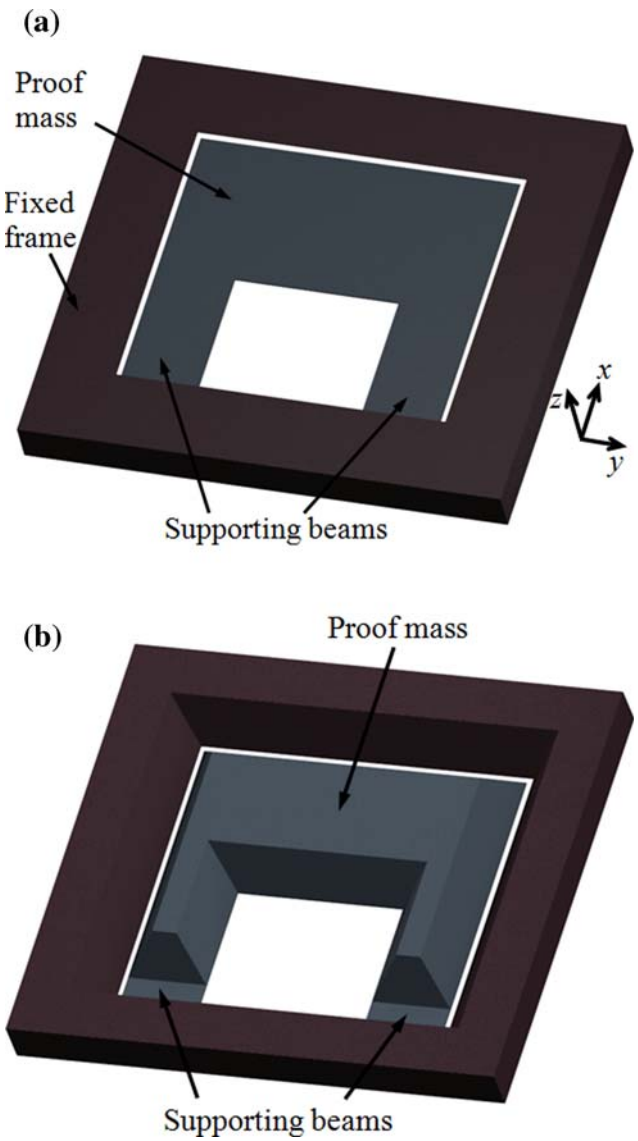

Fig. 1 A 3D schematic view of the (**a**) upper and (**b**) lower parts of the piezoresistive microaccelerometer

2.1 Structural model

Figure 1a and b shows the structural configuration of a piezoresistive microaccelerometer based on cantilever-type beams. The microaccelerometer consists of two supporting beams, a proof mass, a fixed frame, and four piezoresistors in a Wheatstone bridge configuration. An optimization model is used on this microaccelerometer to find the optimum dimensions that improve its bandwidth without exceeding the material rupture stress, while maintaining a high sensitivity. Thus, the proposed optimization model will guarantee safe operation of this kind of microaccelerometer for each specific application.

Figure 2 shows the geometrical parameters used to optimize the dimensions of the structural configuration of the piezoresistive microaccelerometer. Its structural configuration is divided into three elastic beams with three different lengths (L_1, L_2, and L_3), two thicknesses (s_1 and s_2), and two widths (v_1 and v_2). To simplify the optimization model, we propose neglecting the slopes of the proof mass due to anisotropic etching and consider the ends of the supporting beams as clamped ends. In addition, the

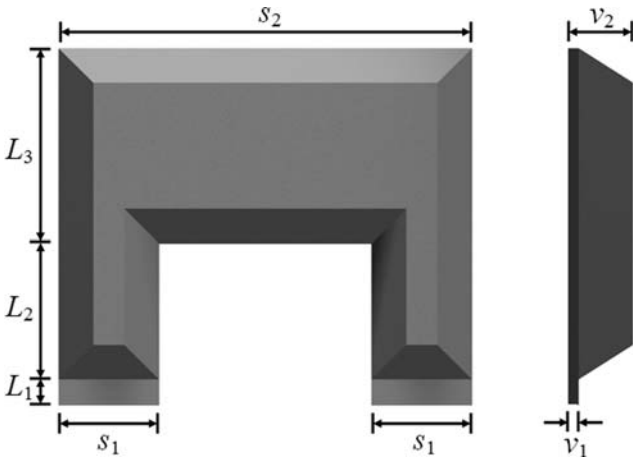

Fig. 2 Geometrical parameters of the structure of the piezoresistive microaccelerometer

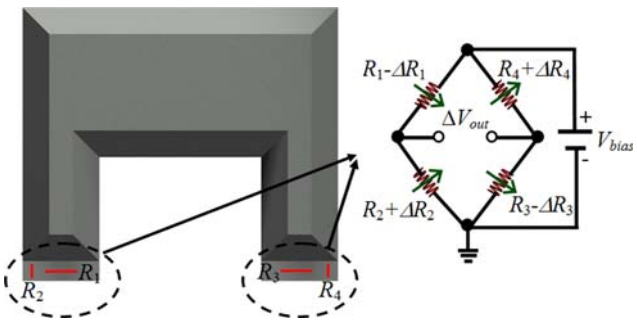

Fig. 3 Localization of the piezoresistive Wheatstone bridge on the structure of the piezoresistive microaccelerometer

thickness of the proof mass is much larger than that of the supporting beams.

When a normal acceleration is applied to the piezoresistive microaccelerometer, its proof mass experiences a vertical deflection that causes transversal and longitudinal strains on the ends of the supporting beams. These strains produce a change in the resistances (R_1, R_2, R_3, and R_4) of each piezoresistor placed on the supporting beams. Thus, these variations cause a change in the output voltage (ΔV_{out}) of the Wheatstone bridge (see Fig. 3). In this configuration, the acceleration magnitude is measured as a function of the output voltage of the Wheatstone bridge.

2.2 Bandwidth modeling

The optimization of bandwidth is needed to widen the application range of the microaccelerometers. This optimization must be achieved while maintaining a suitable sensitivity and low stress level in order to guarantee an efficient and safe operation of the microaccelerometers.

The bandwidth of a microaccelerometer is determined at the first resonant frequency of its structural system (Fraden 1996). The fundamental resonant frequency of a continuous structural system can be obtained using the Rayleigh method. This method is very simple and easier to use than exact analysis for systems with varying distributions of mass and stiffness (Rao 2004). The Rayleigh method calculates the fundamental resonant frequency of a continuous system through the ratio of the expression for potential energy to the expression for kinetic energy in the system (Beards 1995). We use this method to determine the first resonant frequency of the structure of the piezoresistive microaccelerometer. In addition, we consider unit acceleration ($1g$) perpendicular to the normal plane of the structure. This acceleration causes a deflection in the structure of the microaccelerometer, which can be obtained using the Euler–Bernoulli beam theory. Based on this theory, we obtain the following expressions for the bending moments on the microaccelerometer structure (Rao 2004).

$$2EI_1\frac{\partial^2 z_1(x)}{\partial x^2} = -M_1(x), \quad 0 \le x \le L_1, \tag{1}$$

$$2EI_2\frac{\partial^2 z_2(x)}{\partial x^2} = -M_2(x), \quad L_1 \le x \le L_2, \tag{2}$$

$$EI_3\frac{\partial^2 z_3(x)}{\partial x^2} = -M_3(x), \quad L_2 \le x \le L_3, \tag{3}$$

where I_i is the moment of inertia of the i-th beam cross section about the y-axis, $I_1 = s_1 v_1^3/12$, $I_2 = s_1 v_2^3/12$, $I_3 = s_2 v_2^3/12$, E is the elastic modulus, $M_i(x)$ are bending moment functions on the i-th beam, and $z_i(x)$ are the deflection functions of the i-th beam.

The boundary conditions for each beam are given by:

$$\begin{aligned} &z_1(0) = 0, \quad \frac{\partial z_1}{\partial x}(0) = 0, \\ &z_2(0) = z_1(L_1), \quad \frac{\partial z_2}{\partial x}(0) = \frac{\partial z_1}{\partial x}(L_1), \\ &z_3(0) = z_2(L_2), \quad \frac{\partial z_3}{\partial x}(0) = \frac{\partial z_2}{\partial x}(L_2). \end{aligned} \tag{4}$$

With a unit acceleration g, the bending moment functions of each beam are as follows

$$\begin{aligned} M_1(x) = {} & g\rho s_1 v_1 x^2 - g\rho s_2 v_2 L_2 x \\ & - 2g\rho s_1 v_2 L_2 x - 2g\rho s_1 v_1 L_2 x \\ & + \frac{1}{2} g\rho s_2 v_2 L_3^2 + g\rho s_2 v_2 L_2 L_3 \\ & + g\rho s_2 v_2 L_1 L_3 + g\rho s_1 v_2 L_2^2 \\ & + 2g\rho s_1 v_2 L_1 L_2 + g\rho s_1 v_1 L_1^2 \end{aligned} \quad 0 \le x \le L_1, \tag{5}$$

$$M_2(x) = g\rho s_1 v_2 x^2 - g\rho s_2 v_2 L_3 x - 2g\rho s_1 v_2 L_2 x + \frac{1}{2} g\rho s_2 v_2 L_3^2 + g\rho s_2 v_2 L_2 L_3 + g\rho s_1 v_2 L_2^2 \quad L_1 \le x \le L_2, \tag{6}$$

$$M_3(x) = \frac{1}{2} g\rho s_2 v_2 x^2 - g\rho s_2 v_2 L_3 x + \frac{1}{2} g\rho s_2 v_2 L_2^2 \quad L_2 \le x \le L_3. \tag{7}$$

Using the Rayleigh method, the first resonant frequency of the microaccelerometer is determined by the following expression (Rao 2004)

$$f_{res} = \frac{1}{2\pi}\sqrt{\frac{U_{max}}{T_{max}}}, \tag{8}$$

where U_{max} is the maximum potential energy of the microaccelerometer structure and T_{max} is the maximum kinetic energy of the microaccelerometer structure.

$$\begin{aligned} U_{max} = {} & \int_0^{L_1} I_1 E\left(\frac{\partial^2 z_1(x)}{\partial x^2}\right)^2 dx + \int_{L_1}^{L_2} I_2 E\left(\frac{\partial^2 z_2(x)}{\partial x^2}\right)^2 dx \\ & + \frac{1}{2}\int_{L_2}^{L_3} I_3 E\left(\frac{\partial^2 z_3(x)}{\partial x^2}\right)^2 dx, \end{aligned} \tag{9}$$

$$T_{max} = \int_0^{L_1} \rho A_1 z_1^2(x) dx + \int_{L_1}^{L_2} \rho A_2 z_2^2(x) dx + \frac{1}{2}\int_{L_2}^{L_3} \rho A_3 z_3^2(x) dx, \tag{10}$$

where A_i is the cross-section area of the i-th beam.

The functions of deflection $z_1(x)$, z_2(x) and $z_3(x)$ are obtained substituting the Eqs. 1–3 into the boundary conditions given by Eq. 4 (Cortés-Pérez 2008).

$$\begin{aligned} z_1(x) = -\frac{g\rho}{2s_1v_1^3E}(&s_1v_1x^4 - 2s_2v_2L_3x^3 - 4s_1v_2L_2x^3 \\ &- 4s_1v_1L_1x^3 + 3s_2v_2L_3^2x^2 + 6s_2v_2L_2L_3x^2 \\ &+ 6s_1v_2L_2^2x^2 + 12s_1v_2L_1L_2x^2 + 6s_2v_2L_1L_3x^2 \\ &+ 6s_1v_1L_1^2x^2), \end{aligned} \tag{11}$$

$$\begin{aligned} z_2(x) = -\frac{g\rho}{2s_1v_1^3v_2^2E}(&s_1v_1^3x^4 - 4s_1v_1^3L_2x^3 - 2v_1^3s_2L_3x^3 \\ &+ 6s_1v_1^3L_2^2x^2 + 6s_2v_1^3L_2L_3x^2 + 3s_2v_1^3L_3^2x^2 \\ &+ 4s_1v_1v_2^2L_1^3x + 12s_1v_2^3L_1^2L_2x + 12s_1v_2^3L_1L_2^2x \\ &+ 6s_2v_2^3L_1^2L_3x + 12s_2v_2^3L_1L_2L_3x + 6s_2v_2^3L_1L_3^2x \\ &+ 4s_2v_2^3L_1^3L_3 + 3s_1v_1v_2^2L_1^4 + 8s_1v_2^3L_1^3L_2 \\ &+ 6s_1v_2^3L_1^2L_2^2 + 6s_2v_2^3L_1^2L_2L_3 + 3s_2v_2^3L_1^2L_3^2), \end{aligned} \tag{12}$$

$$\begin{aligned} z_3(x) = -\frac{g\rho}{2s_1v_1^3v_2^2E}(&s_1v_1^3x^4 - 4s_1v_1^3L_3x^3 + 6s_1v_1^3L_3^2x^2 \\ &+ 4s_1v_1^3L_2^3x + 12s_1v_2^3L_1L_2^2x + 12s_1v_2^3L_1^2L_2x \\ &+ 4s_1v_1v_2^2L_1^3x + 6s_2v_1^3L_2L_3^2x + 6s_2v_2^3L_1L_3^2x \\ &+ 6s_2v_2^3L_1^2L_3x + 6s_2v_1^3L_2^2L_3x + 12s_2v_2^3L_1L_2L_3x \\ &+ 3s_1v_1v_2^2L_1^4 + 18s_1v_2^3L_1^2L_2^2 + 4s_1v_1v_2^2L_1^3L_2 \\ &+ 4s_2v_1^3L_2^3L_3 + 3s_2v_1^3L_2^2L_3^2 + 3s_1v_1^3L_2^4 + 4s_2v_2^3L_1^3L_3 \\ &+ 12s_2v_2^3L_1^2L_2L_3 + 8s_1v_2^3L_1^3L_2 + 12s_2v_2^3L_1L_2^2L_3 \\ &+ 6s_2v_2^3L_1L_2L_3^2 + 3s_2v_2^3L_1^2L_3^2 + 12s_1v_2^3L_1L_2^3). \end{aligned} \tag{13}$$

To simplify the operations, we propose the following dimensionless geometrical parameters:

$$s = \frac{s_2}{s_1}, \quad v = \frac{v_2}{v_1}, \quad L = \frac{L_2}{L_1}, \quad w = \frac{L_3}{L_1}, \tag{14}$$

Using Eqs. 8–10 and 14, we determined the first resonant frequency or bandwidth of the piezoresistive microaccelerometer (Cortés-Pérez 2008):

$$f_{\text{res}} = \frac{1}{2\pi}\sqrt{\frac{126\,v^2v_1^2E}{\rho L^4}}\sqrt{\frac{A}{B_1 + B_2 + B_3}}, \tag{15}$$

where

$$\begin{aligned} A = {} & 60L^2s^2v^3w^2 + 60Ls^2v^3w^3 + 15s^2v^3w^4 + 120L^3sv^3w \\ & + 30L^2s^3w^3 + 60L^2sv^3w^2 + 60Ls^2v^3w^2 + 30s^2v^3w^3 \\ & + 60L^4v^3 + 20L^3s^2w^2 + 20L^3sw^3 + 180L^2sv^3w \\ & + 15Ls^2w^4 + 60Lsv^3w^2 + 20s^2v^3w^2 + 30L^4sw \\ & + 120L^3v^3 + 80Lsv^3w + 6sw^5 + 12L^5 + 80L^2v^3 \\ & + 40Lsv^2w + 20sv^2w^2 + 40L^2v^2 \\ & + 30sv^2w + 60Lv^2 + 12v \end{aligned}$$

$$\begin{aligned} B_1 = {} & 15120s^3v^6w^4 + 9936s^2v^5w^2 + 1456L^9 + 1456v^3 \\ & + 3780L^2w^7s^3 + 5040L^4w^5s^2 + 3276Lw^8s^2 \\ & + 2268L^4w^5s + 6336L^7sw^2 + 3024L^3w^6s^2 \\ & + 1680L^6w^3s + 15624L^5s^2w^4 + 9936L^7s^2w^2 \\ & + 15120L^5s^3w^4 + 13230L^3w^6s^3 + 2184L^3w^6s \\ & + 19845L^4s^3w^5 + 5544L^2w^7s^2 + 6552L^8sw \\ & + 19656L^6s^2w^3 + 728sw^9 + 13104L^8v^3 + 22176L^7v^3 \\ & + 30240L^7v^6 + 4368L^6v^2 + 105840L^6v^6 + 12096L^6v^3 \\ & + 158760L^5v^6 + 4536L^5v^2 + 20160L^5v^5 \\ & + 120960L^4v^6 + 62496L^4v^5 + 40320L^3v^6 \\ & + 78624L^3v^5 + 3360L^3v^4 + 39744L^2v^5 \\ & + 12672L^2v^4 + 13104Lv^4 + 5040L^6s^3w^3 \\ & + 52416L^7v^3sw + 69552L^6v^3s^2w^2 + 105840L^6v^6sw \\ & + 44352L^6v^3sw^2 + 77616L^6v^3sw + 75600L^5v^6sw^2 \\ & + 36288L^5v^3sw + 317520L^5v^6sw + 10080L^5w^3sv^3 \\ & + 87696L^5v^3s^2w^2 + 57456L^5v^3sw^2 \\ & + 117936L^5v^3s^2w^3 + 120960L^5v^6s^2w^2 \\ & + 13104L^5v^2sw + 30240L^5s^3v^3w^3 \\ & + 12600L^4v^2sw^2 + 78120L^4v^3s^2w^4 + 30240L^4s^3v^3w^3 \\ & + 396900L^4v^6sw + 10080L^4w^3sv^3 + 10080L^4s^2v^2w^2 \\ & + 11340L^4v^2sw + 75600L^4s^3v^3w^4 + 166320L^4v^6s^2w^3 \end{aligned}$$

$$\begin{aligned} B_2 = {} & 128520L^4v^3s^2w^3 + 302400L^4v^6s^2w^2 + 15120L^4w^3sv^6 \\ & + 189000L^4v^6sw^2 + 50400L^4v^5sw + 45360L^4s^3v^6w^3 \\ & + 20160L^4v^3sw^2 + 35280L^4v^3s^2w^2 + 20160L^3s^2v^2w^3 \\ & + 9072L^3w^5sv^3 + 90720L^3s^3v^6w^4 + 40320L^3v^5sw^2 \\ & + 30240L^3s^2v^5w^2 + 20160L^3w^5v^3s^2 + 79380L^3s^3v^3w^5 \\ & + 3360L^3w^3sv^2 + 83160L^3v^6s^2w^4 + 10080L^3s^3v^3w^3 \\ & + 40320L^3v^3s^2w^3 + 309960L^3v^6s^2w^2 + 241920L^3v^6sw \\ & + 173880L^3v^6sw^2 + 332640L^3v^6s^2w^3 + 124992L^3v^5sw \\ & + 90720L^3s^3v^6w^3 + 30240L^3w^3sv^6 + 7560L^3v^2sw^2 \\ & + 73080L^3v^3s^2w^4 + 60480L^3s^3v^3w^4 + 7560L^3s^2v^2w^2 \\ & + 11340L^2s^2v^2w^3 + 13608L^2w^5sv^3 + 136080L^2s^3v^6w^4 \\ & + 72576L^2v^5sw^2 + 57456L^2s^2v^5w^2 + 15120L^2w^5v^3s^2 \\ & + 47250L^2s^3v^3w^5 + 16380L^2s^2w^4v^2 + 39690L^2w^6s^3v^3 \\ & + 15120L^2w^5v^6s^2 + 124740L^2v^6s^2w^4 + 151200L^2v^6s^2w^2 \\ & + 60480L^2v^6sw + 60480L^2v^6sw^2 + 238140L^2v^6s^2w^3 \\ & + 117936L^2v^5sw + 75600L^2s^3v^6w^3 + 15120L^2w^3sv^6 \\ & + 15120L^2v^3s^2w^4 + 15120L^2s^3v^3w^4 + 71820L^2s^3v^6w^5 \end{aligned}$$

$$
\begin{aligned}
B_3 = {} & 45360L^2s^2v^5w^3 + 9072L^2w^6s^2v^3 + 10080L^2w^3sv^5 \\
& + 5040L^2sv^4w + 6552L^2w^6sv^3 + 6048Lw^5sv^3 \\
& + 75600Ls^3v^6w^4 + 39312Lv^5sw^2 + 39312Ls^2v^5w^2 \\
& + 7560Ls^3v^3w^5 + 5670Ls^2w^4v^2 + 13230Lw^6s^3v^3 \\
& + 15120Lw^5v^6s^2 + 47250Lv^6s^2w^4 + 30240Lv^6s^2w^2 \\
& + 60480Lv^6s^2w^3 + 39744Lv^5sw + 30240Ls^3v^6w^3 \\
& + 5040Lsv^4w^2 + 71820Ls^3v^6w^5 + 57456Ls^2v^5w^3 \\
& + 9072Lw^6s^2v^3 + 10080Lw^3sv^5 + 12672Lsv^4w \\
& + 6552Lw^6sv^3 + 11088Lw^7s^2v^3 + 26460Lw^6s^3v^6 \\
& + 5040Lw^5s^2v^2 + 25200Ls^2v^5w^4 + 7560Lw^7s^3v^3 \\
& + 3024Lw^5sv^2 + 5040s^3v^6w^3 + 5040w^5s^2v^5 \\
& + 6336sv^4w^2 + 3780w^7s^3v^6 + 2184w^6sv^2 \\
& + 3276w^8s^2v^3 + 1680w^3sv^4 + 19845s^3v^6w^5 \\
& + 19656s^2v^5w^3 + 3024w^6s^2v^3 + 6552sv^4w \\
& + 5544w^7s^2v^3 + 13230w^6s^3v^6 + 15624s^2v^5w^4 \\
& + 2268w^5sv^2
\end{aligned}
$$

Therefore, the bandwidth of the piezoresistive microaccelerometer can be determined through Eq. 15.

2.3 Sensitivity modeling

The sensitivity of a piezoresistive microaccelerometer is here defined as the relative change of resistance, R, of the piezoresistors per unit of acceleration g (Seidel and Csepregi 1984):

$$S = \frac{\Delta R}{Rg}, \tag{16}$$

where ΔR is the change of resistance of the piezoresistors.

Assuming uniform stresses within the piezoresistor, the resistance change due to biaxial stress is given by (Senturia 2002):

$$\frac{\Delta R}{R} = \pi_l\sigma_l + \pi_t\sigma_t, \tag{17}$$

where π_l and π_t are the longitudinal and the transverse piezoresistance coefficients, and σ_l and σ_t are the longitudinal and the transverse stresses, respectively.

In Eq. 17 the shear effects are neglected due to their small contribution compared to the longitudinal and transverse stresses. The longitudinal direction is parallel to the current flow in the piezoresistor, while the transverse is orthogonal to it. The two coefficients are dependent on the crystal orientation and doping (p-type or n-type), and concentration of the piezoresistors. For p-type [110] oriented piezoresistors and deposited on a silicon ⟨100⟩ wafer, the piezoresistive coefficients π_{11} and π_{12} are much smaller than π_{44} (Senturia 2002). Thus in this case, an approximation for the change of resistance is obtained as:

$$\frac{\Delta R}{R} \cong \frac{\pi_{44}}{2}(\sigma_l - \sigma_t), \tag{18}$$

where π_{44} is the shear piezoresistance coefficient.

Substituting Eq. 18 into 16, the sensitivity of piezoresistive microaccelerometers as a function of the longitudinal and transverse stresses is determined by:

$$S \cong \frac{\pi_{44}}{2g}(\sigma_l - \sigma_t). \tag{19}$$

For thin cantilever-type beams with small deflections, the transverse stress can be neglected to simplify the sensitivity equation (Duc et al. 2006). Therefore,

$$S \cong \frac{\pi_{44}}{2g}\sigma_l, \tag{20}$$

where the maximum longitudinal stress is closed to the clamped end of cantilever, which is determined by

$$\sigma_l = \frac{Mc}{I}, \tag{21}$$

where M is the bending moment, c is the distance between the neutral plane of the beam to the position of the piezoresistor, and I is the moment of inertia of the beam cross section about the y axis.

For the beam end ($x = 0$), the bending moment is calculated with Eq. 5. Substituting it into Eqs. 20, 21 and considering the dimensionless geometrical parameters, we obtain the sensitivity in terms of L, s, v, w, L_1 and v_1.

$$S \cong \frac{\pi_{44}}{2}\frac{3g\rho L_1^2}{2v_1}(2 + 4vL + 2vL^2 + 2svw + 2svwL + svw^2). \tag{22}$$

This equation is very important in the calculation of the approximate sensitivity of the piezoresistive microaccelerometer with two cantilever-type beams and a proof mass.

2.4 Stress modeling

Most piezoresistive microaccelerometers have a structural configuration based on silicon, which is a brittle material. Therefore, a failure criterion of this material must be based on brittle materials. Thus, we propose to use the maximum-normal-stress failure theory to predict the mechanical failure of the silicon structure of the piezoresistive microaccelerometer. This theory assumes that a brittle material will fail when the principal stresses (σ_i) are higher than the rupture stress (σ_u) of the material (Norton 2006).

For the proposed microaccelerometer, a normal acceleration of n-times g causes a maximum longitudinal stress on the supporting beams ends, which is n times larger than Eq. 21. The maximum bending moment on the supporting beam is

obtained substituting $x = 0$ into Eq. 5. Thus, the principal stress can be approximated to the maximum longitudinal stress, which is determined by (Cortés-Pérez 2008):

$$\sigma_{\max} = \frac{3ng\rho}{2v_1^3}\left(s_2v_2L_3^2 + 2s_2v_2L_2L_3 + 2s_2v_2L_1L_3 + 2s_1v_2L_2^2 + 4s_1v_2L_1L_2 + s_1v_1L_1^2\right). \quad (23)$$

Substituting Eq. 23 into equation of maximum-normal-stress failure theory (Norton 2006) and considering the safety factor, F, of the structure, we obtained the constraint of the maximum stress in terms of the geometrical parameters of the piezoresistive microaccelerometer.

$$\frac{3ng\rho}{2v_1^3}\left(s_2v_2L_3^2 + 2s_2v_2L_2L_3 + 2s_2v_2L_1L_3 + 2s_1v_2L_2^2 + 4s_1v_2L_1L_2 + s_1v_1L_1^2\right) \le \frac{\sigma_u}{F}. \quad (24)$$

Substituting Eq. 14 into 23, we obtain the maximum normal stress as a function of L, s, v, w, L_1 and v_1.

$$\sigma_{\max} = \frac{3ng\rho L_1^2}{2v_1}(2 + 4vL + 2vL^2 + 2svw + 2svwL + svw^2). \quad (25)$$

3 Structural parameter sensitivity

In this section, the variations of the bandwidth, sensitivity, and maximum normal stress of the piezoresistive microaccelerometer in terms of its geometrical parameters are studied. The end result of this study is to find the geometrical parameters that have the most influence on the bandwidth, sensitivity, and the maximum normal stress of the microaccelerometer. Thus, this study helps designers to predict the effect on the microaccelerometer performance when the structural dimensions are modified. Therefore, we considered four geometrical parameters (L, s, v, and w) and derived the bandwidth, sensitivity, and maximum normal stress with respect to each parameter. In case of the bandwidth, its variation in relation to each geometrical parameter is given by:

$$f_P \equiv \frac{\partial f}{\partial P} = \frac{1}{2\pi}\sqrt{\frac{126v_1^2E}{\rho}}F_P(L, s, v, w), \quad (26)$$

where P represents each geometrical parameter (L, s, v, and w), and $F_P(L, s, v, \text{and } w)$ is the mathematical expression that contain the terms L, s, v, and w, which is obtained taking partial derivative of the bandwidth with respect to each geometrical parameter.

The variations of the sensitivity as a function of each dimensionless geometrical parameter are obtained deriving the equation of sensitivity (Eq. 22) with respect to each dimensionless geometrical parameter: L, s, v, and w (Cortés-Pérez 2008).

In addition, the variations of the maximum normal stress in relation to each dimensionless geometrical parameter are calculated deriving the equation of maximum longitudinal stress (Eq. 25) with respect to each dimensionless geometrical parameter: L, s, v, and w (Cortés-Pérez 2008).

We considered a piezoresistive microaccelerometer based on silicon with the following properties: elasticity modulus of 130 GPa, Poisson ratio of 0.28, and density of 2300 kg/m^3. Thus, the dimensionless geometrical parameter L is a significant parameter for the bandwidth expressions, sensitivity and maximum normal stress of the piezoresistive microaccelerometer. The variations of the bandwidth with respect to each dimensionless geometrical parameter (L, s, v, and w) are showed in Fig. 4. These responses are obtained using Eq. 26 and where $f_L \equiv \partial f/\partial L, f_s \equiv \partial f/\partial s, f_v \equiv \partial f/\partial v$, and $f_w \equiv \partial f/\partial w$. We observed that the responses of the derivatives of the bandwidth with respect to w and L present significant changes when L is increased.

Figure 5 shows the response of the partial derivatives of the sensitivity with respect to each dimensionless geometrical parameter (L, s, v, and w), when the parameter L is increased. For this condition, the responses of the derivatives of the sensitivity with respect to s and w have the greatest variations. Also, Fig. 6 shows the response of the partial derivatives of the maximum normal stress based on each dimensionless geometrical parameter (i.e., $Esf_L \equiv \partial\sigma_{\max}/\partial L$, $Esf_s \equiv \partial\sigma_{\max}/\partial s$, $Esf_v \equiv \partial\sigma_{\max}/\partial v$, and $Esf_w \equiv \partial\sigma_{\max}/\partial w$). For the case of a maximum value L, the derivates of the maximum normal stress with respect to s and w have the greatest variations.

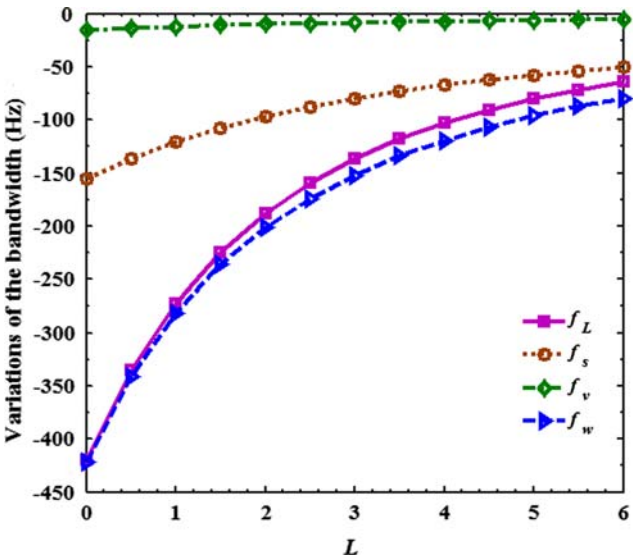

Fig. 4 Variations of the bandwidth as a function of the dimensionless geometrical dimensions L, s, v and w

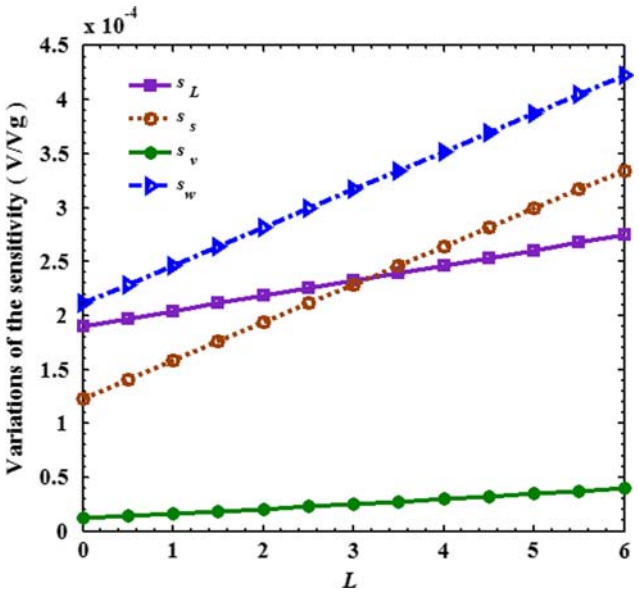

Fig. 5 Variations of the sensitivity as a function of the dimensionless geometrical dimensions L, s, v and w

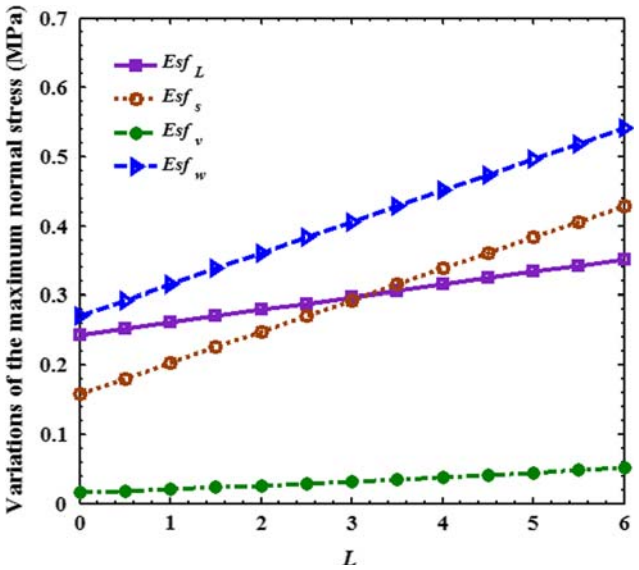

Fig. 6 Variations of the normal stress as a function of the dimensionless geometrical dimensions L, s, v and w

4 Optimization model

The optimization model of the piezoresistive microaccelerometer has the bandwidth as the objective function and the geometrical parameters as the design variables. Their constraints include performance parameters such as the sensitivity and the maximum normal stress of the microaccelerometer. In addition, this model considers constraints defined by geometrical parameters that depend of the structural configuration and the fabrication process. Two structural configurations of piezoresistive microaccelerometers are optimized to support $10g$ and $50g$ accelerations.

4.1 Design variables

The design variables are defined by the structural configuration of the piezoresistive microaccelerometer. For this case, Fig. 2 shows the design variables of the optimization model that includes the geometrical parameters such as s_1, s_2, v_1, v_2, L_1, L_2, and L_3.

4.2 Limitations–constraints

The constraints may be classified as explicit and implicit constraints. The explicit constraints restrict the range of the design variables and the implicit constraints consider the performance requirements. For this case, the implicit constraints are integrated by the sensitivity and normal stress of the piezoresistive microaccelerometer. Moreover, the explicit constraints are given by the bounds of the dimensions (s_1, s_2, v_1, v_2, L_1, L_2, and L_3) of the piezoresistive microaccelerometer, as shown in Table 1.

The performance requirements (implicit constraints) include sensitivity compared with that of the microaccelerometer reported by Plaza et al. (2002) and a model JTF commercial accelerometer fabricated by the Honeywell Company (http://content.honeywell.com/sensing/sensotec/pdf_catalog08/008727-1-EN_Model_JTF_Gen_Pur.pdf accessed 16 July 2009). In addition, these requirements consider a maximum normal stress given by the silicon rupture stress divided by a safety factor of 1.5. Table 2 shows the performance requirements of the proposed optimization model for two structural configurations of piezoresistive microaccelerometers.

4.3 Problem formulation

The mathematical representation of the optimization problem is the maximization of the objective function

Table 1 Explicit constraints for the proposed optimization model

Bounds	s_1 (μm)	v_1 (μm)	L_1 (μm)	s_2 (μm)	v_2 (μm)	L_2 (μm)	L_3 (μm)
Lower	200	10	200	2500	350	500	1000
Upper	1200	45	1200	3500	450	1200	2500

Table 2 Performance requirements for the proposed optimization model

Performance requirements	Structure 1 ($10g$)	Structure 2 ($50g$)
$S_{\min}$ (mV/Vg)	1.03	0.16
$\sigma_{\max} = \frac{\sigma_u}{F}$ (GPa)	0.44	0.44

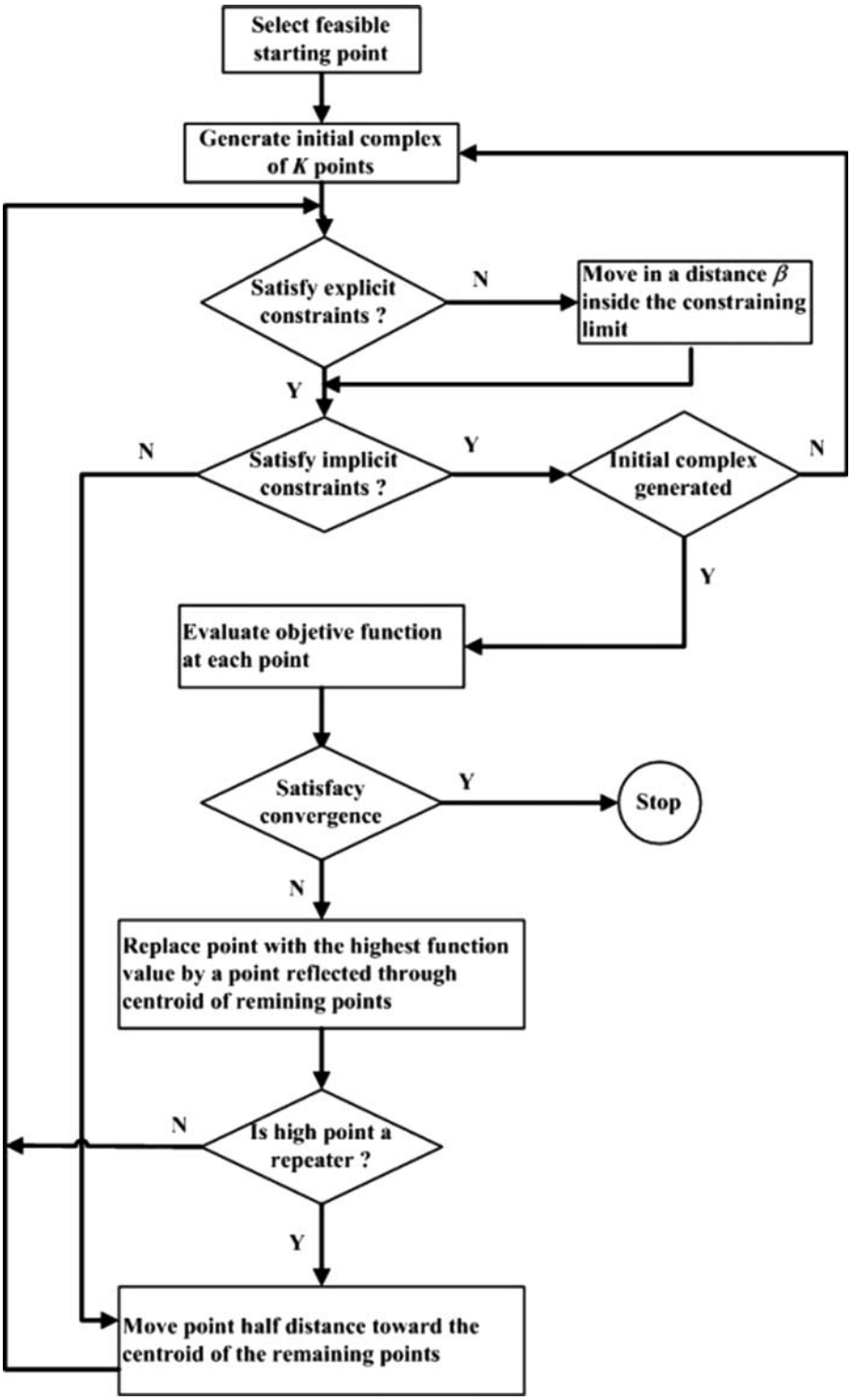

Fig. 7 Flow diagram of the Box-Complex method used to solve the proposed optimization model

denoted as F($\boldsymbol{x}$). In this case, the objective function is the bandwidth of the piezoresistive microaccelerometer. As the Box-Complex method finds the minimum of an objective function, we change the sign of the objective function to maximize it through this method. Hence the optimization problem is given by:

$$\text{Minimize } F(\boldsymbol{x}) = -f_{\text{res}}$$

such that

$$\frac{3\rho g}{2v_1^3}\frac{\pi_{44}}{2}\left(s_2v_2L_3^2 + 2s_2v_2L_2L_3 + 2s_2v_2L_1L_3 + 2s_1v_2L_2^2 + 4s_1v_2L_1L_2 + s_1v_1L_1^2\right) \geq S_a$$

$$\frac{3ng\rho}{2v_1^3}\left(s_2v_2L_3^2+2s_2v_2L_2L_3+2s_2v_2L_1L_3+2s_1v_2L_2^2 +4s_1v_2L_1L_2+s_1v_1L_1^2\right)\le\frac{\sigma_u}{F}$$

$$\begin{aligned}
&200\le s_1\le 1200\\
&10\le v_2\le 45\\
&200\le L_1\le 1200\\
&2500\le s_2\le 3500\\
&350\le v_2\le 450\\
&500\le L_2\le 1200\\
&1000\le L_3\le 2500,
\end{aligned} \tag{27}$$

where f_{res} is the bandwidth of the piezoresistive microaccelerometer, S_a is the adequate value of the sensitivity of the microaccelerometer for an specific application (this magnitude must be chosen high for optimum performance), σ_u is the rupture stress of the material of the microaccelerometer.

4.4 Box-Complex method implementation

The Box-Complex method is used to maximize the bandwidth of the piezoresistive microaccelerometer. This method takes advantages of being an easy algorithm and considers implicit and explicit constraints. In addition, this method is a constrained minimization technique that uses a random search and does not require derivatives of the objective function (Farkas and Jármai 1997). The method is applied to nonlinear programming problems with inequality constraints. Here the Box-Complex method was used to determine the optimum dimensions of the piezoresistive microaccelerometer to maximize its bandwidth keeping high sensitivity and a normal stress less than the rupture stress of the silicon. An algorithm, based on the Box-Complex method was developed using the Matlab software for a maximum error of 0.1%. Figure 7 shows the flow diagram of the Box-Complex method used in this work.

The Box-Complex method uses a polyhedron (called complex) with more than $(n + 1)$ vertices, being n the number of design variables. This complex moves around the solution space through expansion and contraction. In the first iteration cycle an original complex is generated, where the complex contains $K \ge n + 1$ feasible points or vertices in an n-dimensional design space. It considered that at least one initial feasible point exists, which is called the starting point and the remaining $(K-1)$ points are generated randomly. Next, the algorithm examines whether the initial point satisfies the explicit constraints. If not, it is moved a small distance β inside the constraining limit. Now, the algorithm checks whether the point satisfies the implicit constraints. If an implicit constraint is violated, the

Table 3 Design variables and performance requirements optimized for two structures of piezoresistive microaccelerometers

Microaccelerometer	s_1 (μm)	v_1 (μm)	L_1 (μm)	s_2 (μm)	v_2 (μm)	L_2 (μm)	L_3 (μm)	Normal stress (MPa)	Sensitivity (mV/Vg)	Bandwidth (Hz)
1	805	15	200	3305	450	1090	1570	20.31	1.58	569.23
2	800	45	200	3500	450	1000	1595	11.54	0.18	2959.33

Table 4 Comparison of the sensitivity and bandwidth of the microaccelerometer developed by Plaza et al. (2002) and the model JTF accelerometer (code GN) of Honeywell Company (http://content.honeywell.com/sensing/sensotec/pdf_catalog08/008727-1-EN_Model_JTF_Gen_Pur.pdf, accessed 16 July 2009) with those obtained using the proposed optimization model

Performance parameters	10g		50g	
	Microaccelerometer Plaza et al. (2002)	Optimized microaccelerometer 1	Accelerometer (model JTF) Honeywell	Optimized microaccelerometer 2
Sensitivity (mV/Vg)	1.03	1.58	0.16	0.18
Bandwidth (Hz)	326	569.23	2,000	2,959.33

Table 5 Geometrical dimensions of the two microaccelerometers used in the FE models

Microaccelerometer	Geometrical dimensions						
	s_1 (μm)	v_1 (μm)	L_1 (μm)	s_2 (μm)	v_2 (μm)	L_2 (μm)	L_3 (μm)
1	805	15	200	3305	450	1090	1570
2	800	45	200	3500	450	1000	1595

point is moved halfway towards the centroid of the previous points, and the explicit and implicit constraints are evaluated again. Later, the objective function (bandwidth of the microaccelerometer) is evaluated at each of the previous points. Thus, the points with the worst and the best function are determined. After that, if the difference between the worst and best function is less than a tolerance previously established, the solution is found. If this condition is not satisfied, the worst point is rejected from the centroid and replaced with a new one. This new point is examined to determine if it satisfies the explicit constraints. If these explicit constraints are satisfied then the algorithm checks the other implicit constraints. If the new point satisfies the implicit constraints and the objective function value is less than the worst value, then this new point is considered as an improvement.

In the next iteration, if either the function value of the new point is larger than the worst value or any of the implicit constraints are violated, then the algorithm moves this point halfway towards the centroid of the previous points. If this point satisfies the explicit and implicit constraints, but it remains as the worst, then another point must be determined. For this, the algorithm moves the point halfway towards the centroid of the previous points. This process continues until the convergence criterion is

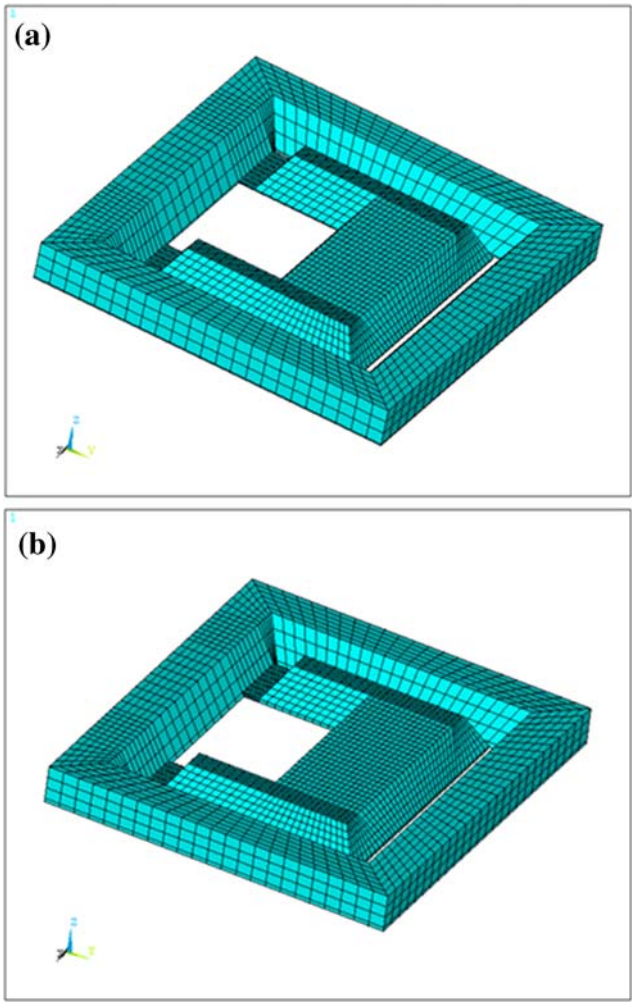

Fig. 8 FE models of the (**a**) first and (**b**) second optimized piezoresistive microaccelerometer

Table 6 First five resonant frequencies of the two FE models of the piezoresistive microaccelerometers

Mode shapes	Microaccelerometer	
	1	2
	Resonant frequency (Hz)	
1	660.9	3119
2	23407	53027
3	53480	95242
4	70634	161190
5	173301	248950

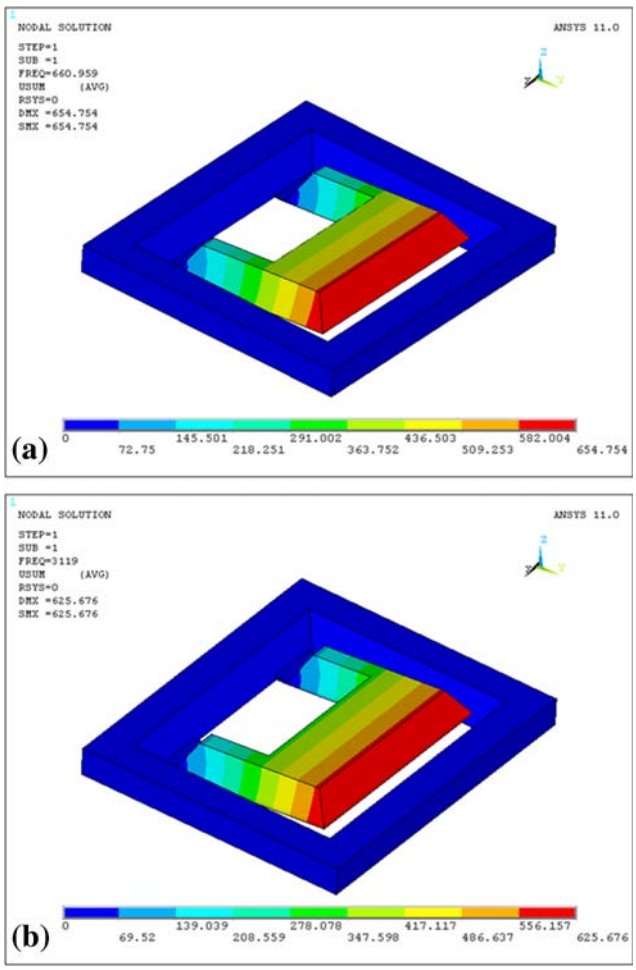

Fig. 9 First mode shape of the (**a**) first and (**b**) second optimized piezoresistive microaccelerometer

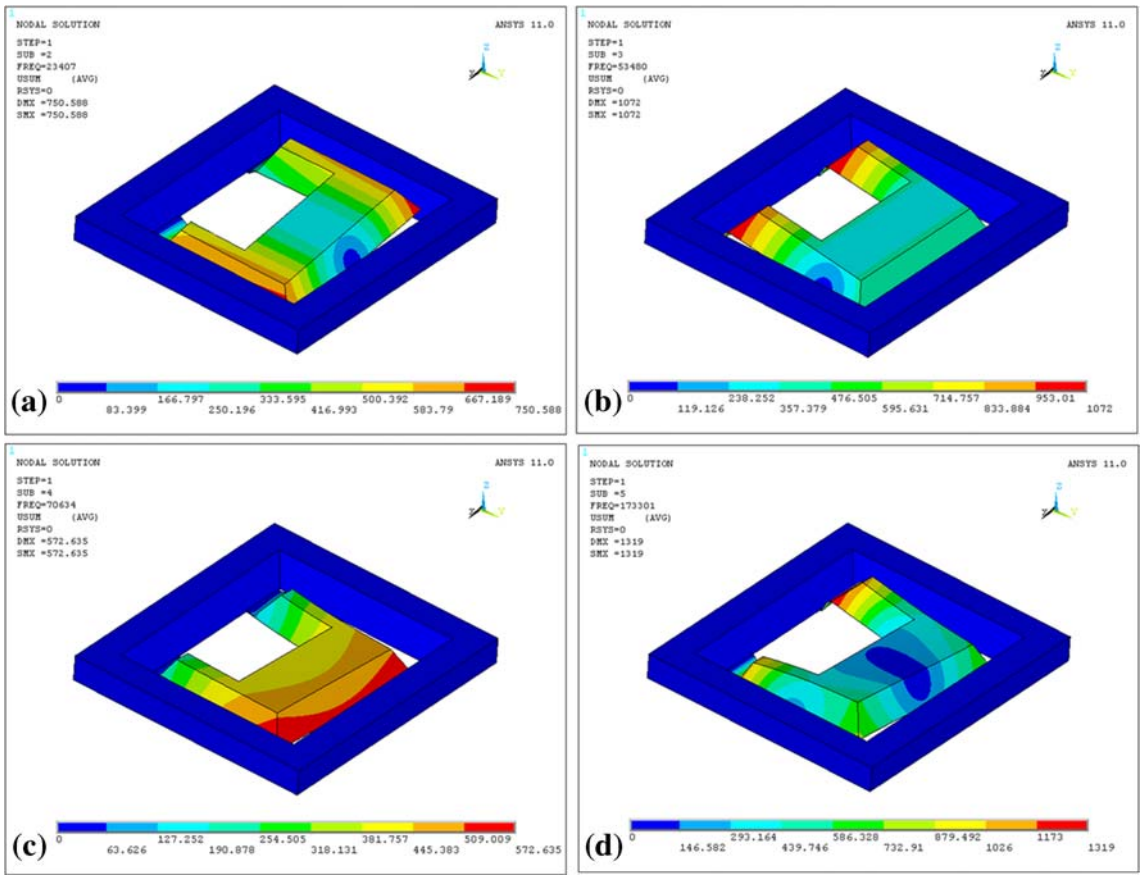

Fig. 10 (**a**) Second, (**b**) third, (**c**) fourth, and (**d**) fifth modal shapes of the first optimized piezoresistive microaccelerometer

satisfied (i.e., the difference between the worst and best function is less than a given tolerance).

In the Box-Complex method, the expansion and contraction of the complex permits it to move closer to the optimal values of the objective function.

5 Results and discussions

Table 3 shows the results of the proposed optimization model using the Box-Complex method for the two structures of the piezoresistive microaccelerometers. The first and second structures were optimized for 10*g* and 50*g* accelerations, respectively. The two structures operate safety for these accelerations since the normal stresses are less than the rupture stress of the silicon, which is presumed to be 360 MPa in silicon ⟨100⟩ wafer (Borky 1997). Table 4 shows the comparison of the structures optimized against the microaccelerometer proposed by Plaza et al. (2002) and the model JTF accelerometer (code GN) of Honeywell Company (http://content.honeywell.com/sensing/sensotec/pdf_catalog08/008727-1-EN_Model_JTF_ Gen_Pur.pdf, accessed 16 July 2009).

For the first optimized microaccelerometer, the bandwidth was increased 74.6% and the sensitivity was improved by 53.4% with respect to the microaccelerometer developed by Plaza et al. (2002). In addition, the second optimized microaccelerometer presented an improvement in the bandwidth and sensitivity of 48.0 and 12.5%, respectively, compared to the model JFT accelerometer fabricated by Honeywell Company (http://content.honeywell.com/sensing/sensotec/pdf_catalog08/008727-1-EN_Model_JTF_ Gen_Pur.pdf, accessed 16 July 2009).

Through the optimization model proposed in this work, the results of the bandwidth, sensitivity and normal stress of the piezoresistive microaccelerometer based on cantilever-type beams can be significantly improved. In addition, this model can be easily solved using the Box-Complex method.

In addition, we developed two FE models using ANSYS software. These FE models help to understand the bandwidth, sensitivity and maximum normal stress of the two piezoresistive microaccelerometers. In these models we considered a horizontal angle of 54.7° on the beams as obtained by the etching process of the microaccelerometer. Table 5 shows the optimum dimensions of the two microaccelerometers used in the FE models.

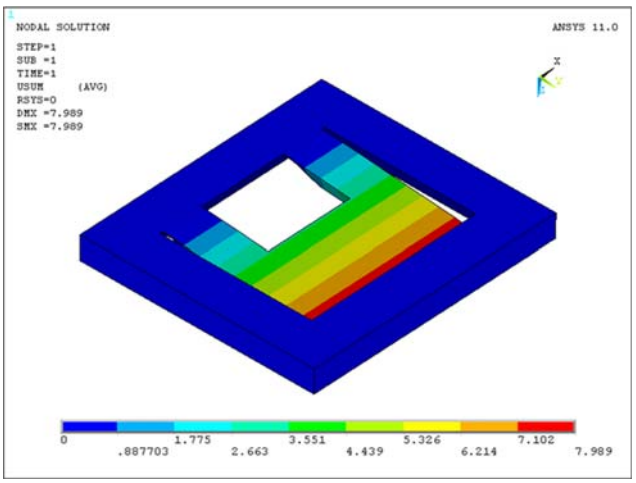

Fig. 11 Deflection distributions (μm) of the first optimized piezoresistive microaccelerometer

Figure 8 shows the FE models of the first and second structure of the microaccelerometers, respectively. In the first and second structure 8,792 and 8,496 finite elements respectively were used. In the supporting beams a fine mesh was used since these zones can be subjected to high stresses. Later, the first five resonant frequencies of each structure were obtained, as shown in Table 6. The first resonance frequency defines the bandwidth of each structure. Figure 9 shows the first mode shape of the two microaccelerometers, with a bandwidth of 660.9 and 3,119 Hz, respectively. These bandwidths have a relative difference of 16.1 and 5.4% with respect to those of the optimization model. These differences are probably caused because the FE models consider the slope of the beams, which are the result of the etching process of the microaccelerometer. In addition, Fig. 10 shows the second, third, fourth and fifth modal shapes of the first microaccelerometer. The first

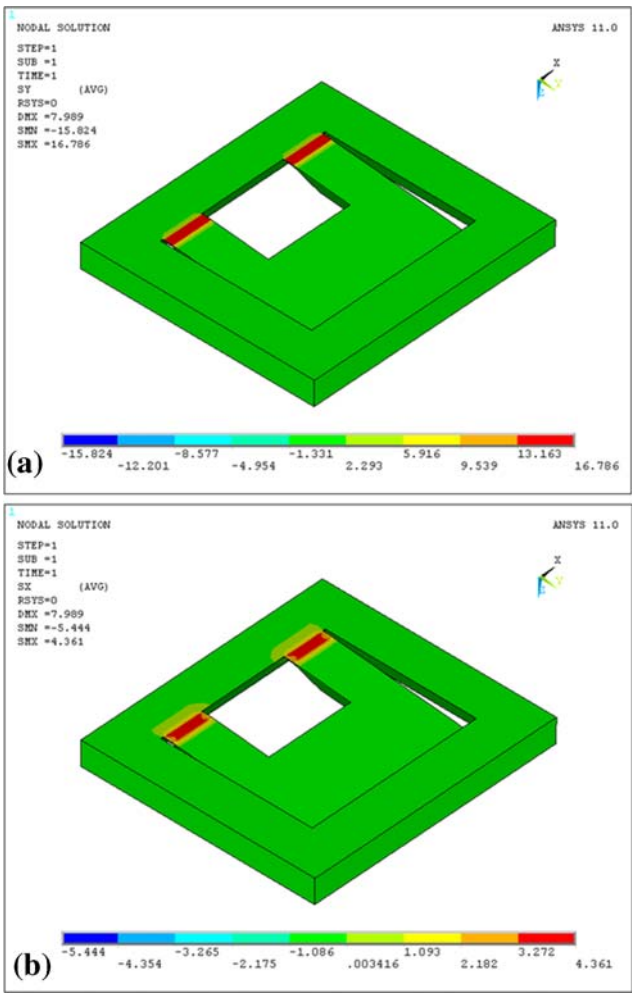

Fig. 12 3D View of the (**a**) longitudinal and (**b**) transverse stress distribution on the first optimized piezoresistive microaccelerometer

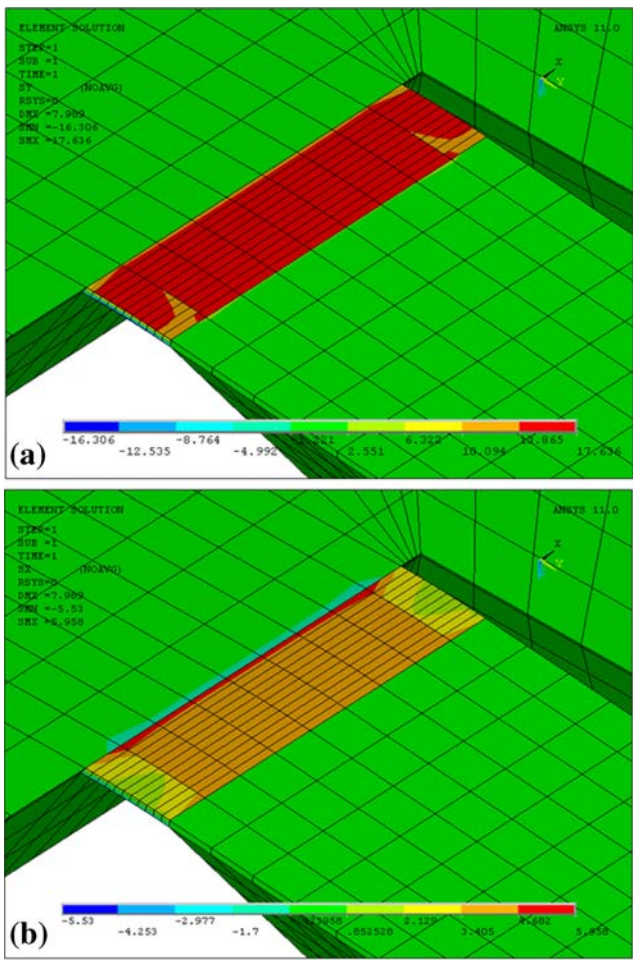

Fig. 13 3D View of the (**a**) longitudinal and (**b**) transverse stress distribution on the supporting beams of the first optimized piezoresistive microaccelerometer

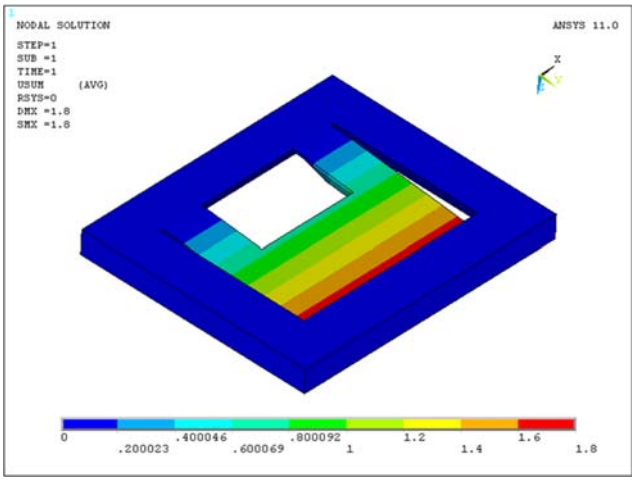

Fig. 14 Deflection distributions (μm) of the second optimized piezoresistive microaccelerometer

mode shape is a bending mode, the second mode is twisting, and the third mode is a lateral type mode.

Next, 10*g* acceleration was applied in the normal direction to the first microaccelerometer. The maximum deflection of this microaccelerometer (7.99 μm) is located at the end of its proof mass, as shown in Fig. 11. This deflection is less than the minimum dimension of the structure of the first microaccelerometer. In addition, the longitudinal and transverse stress distribution on the first microaccelerometer is shown in Fig. 12. Also, Fig. 13 shows the longitudinal and transverse stress distribution on the supporting beams where the piezoresistors (elements 3355 and 3408) will be placed. The maximum transverse and longitudinal stress (on the elements 3355 and 3408) registered 1.69 MPa and 17.61 MPa, respectively. The longitudinal stress obtained with the FE model has a

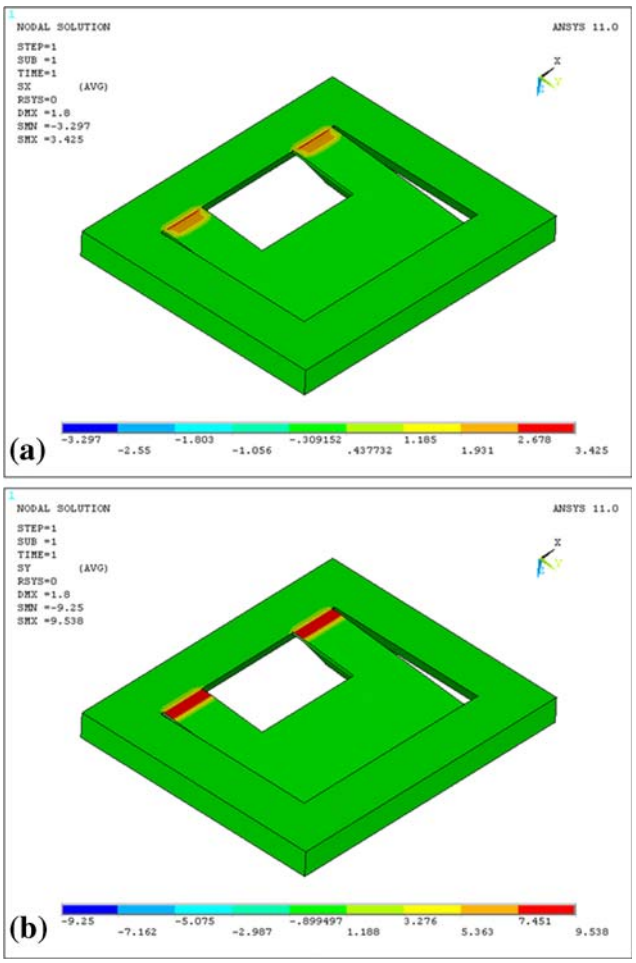

Fig. 15 3D View of the (**a**) transverse and (**b**) longitudinal stress distribution on the second optimized piezoresistive microaccelerometer

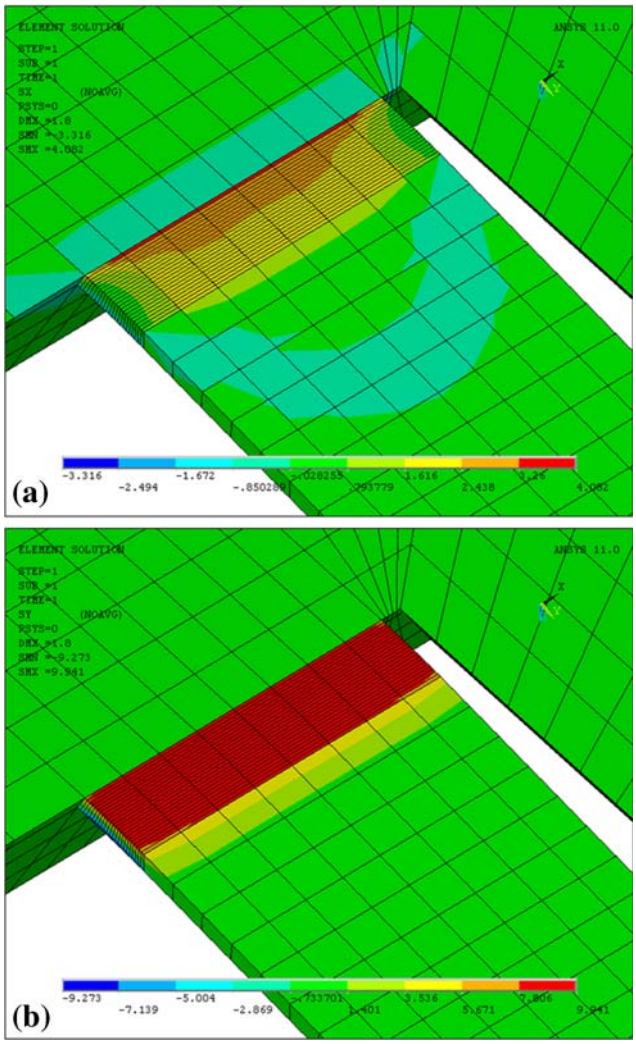

Fig. 16 3D View of the (**a**) transverse and (**b**) longitudinal stress distribution on the supporting beams of the second optimized piezoresistive microaccelerometer

relative difference of −13.3% with respect to that obtained using the optimization model.

The second microaccelerometer was subjected to 50*g* acceleration and it had a maximum deflection of 1.8 μm (see Fig. 14). In addition, Figs. 15 and 16 show the transverse and longitudinal stress distribution on the structure and supporting beams of the second microaccelerometer. In the locations where the piezoresistors (elements 8953 and 9040) will be located, the highest transverse and longitudinal stress (on the elements 8953 and 9040) was 0.27 and 9.94 MPa, respectively. The maximum transverse stress represents 2.7% of the highest longitudinal stress. These values are less than the rupture stress of a silicon ⟨100⟩ wafer (Borky 1997). This longitudinal stress represents a relative difference of −13.9% with respect to that of the optimization model. The two FE models indicated results close to those of the optimization model. In addition, the results of the FE models show that the transverse stresses are much less with respect to the longitudinal stresses. These FE models predict the mechanical behavior of the piezoresistive microaccelerometers.

6 Conclusions

An optimization model to maximize the bandwidth of uniaxial piezoresistive microaccelerometers based on cantilever-type beams was presented. This model used the sensitivity and the maximum normal stress as implicit constraints, which were obtained using the Euler–Bernoulli beam and maximum-normal-stress failure theories. The objective function of the microaccelerometer bandwidth was determined using the Rayleigh method and maximized through an algorithm based on the Box-Complex method. The optimization model was used on a silicon piezoresistive microaccelerometer reported in the literature and subjected to 10*g* and 50*g* accelerations, respectively. This model determined the optimum geometrical dimensions of the microaccelerometer that maximize the bandwidth keeping a high sensitivity and normal stress less than the silicon rupture stress. The results of the optimization model showed a significant increment in the bandwidth and sensitivity of the microaccelerometer, and with normal stress levels that guarantee a safe behavior of its structure. In addition, FE models using the ANSYS software were built to evaluate the mechanical behavior of the optimized microaccelerometers. The results of the FE models agreed well with respect those of the optimization model.

Microaccelerometers with optimum performance are needed in new applications such as biomedical activity monitoring, headsets for virtual reality, computer peripherals and navigation. Future research directions will include minimization of the thermal noise on piezoresistive microaccelerometers. Also, the effect of the residual stress on the structure of the microaccelerometer will be considered.

Acknowledgments This work was supported by the University of Guanajuato (UG DAIP project 099/2008) and CONACYT through project 84605. The valuable discussions and contributions by Professor Jerry Hemmye of Western Michigan University are gratefully acknowledged.

References

Amarasinghe R, Dao DV, Toriyama T, Sugiyama S (2007) Development of miniaturized 6-axis accelerometer utilizing piezoresistive sensing elements. Sens Actuators A 134:310–320. doi:10.1016/j.sna.2006.05.044

Beards CF (1995) Engineering vibration analysis with application to control systems. Edward Arnold, UK

Beeby S, Ensell G, Kraf M, White N (2004) MEMS mechanical sensors. Artech House Inc., Norwood

Borky JM (1997) Silicon diaphragm pressure sensors with integrated electronics. Ph.D. dissertation, University of Michigan, Ann Arbor

Chae J, Kulah H, Najafi K (2005) A monolithic three-axis micro-g micromachined silicon capacitive accelerometer. J Microelectromech Syst 14:235–242. doi:10.1109/JMEMS.2004.839347

Cortés-Pérez AR (2008) Design and optimization of uniaxial microaccelerometer. Master thesis, Guanajuato University, Guanajuato, Mexico (Translation of Spanish thesis)

Coultate JK, Fox CHJ, McWilliam S, Malvern AR (2008) Application of optimal and robust design methods to a MEMS accelerometer. Sens Actuators A 142:88–96. doi:10.1016/j.sna.2007.04.033

Dauderstädt UA, Sarro PM, French PJ (1998) Temperature dependence and drift of a thermal accelerometer. Sens Actuators A 66:244–249

Duc TC, Creemer JF, Sarro PM (2006) Lateral nano-Newton force-sensing piezoresistive cantilever for microparticle handling. J Micromech Microeng 16:S102–S106. doi:10.1088/0960-1317/16/6/S16

Farkas J, Jármai K (1997) Analysis and optimum design of metal structures. Balkema Publishers, Rotterdam

Fedder GK, Chae J, Kulah H, Najafi K, Denison T, Kuang J, Lewis S (2005) Monolithically integrated inertial sensors. In: Baltes H, Brand O, Fedder GK, Hierold C, Korvink J, Tabata O (eds) Advanced Micro & Nanosystems, vol 2. CMOS-MEMS. Wiley-VCH, Weinheim, pp 137–192

Fraden J (1996) Handbook of modern sensors. Springer, New York

Herrera-May AL, Cortés-Pérez AR, Aguilera-Cortés LA (2008) Microaccelerometers: present. Acta Universitaria 18:24–32 Translation of Spanish paper

Herrera-May AL, García-Ramírez PJ, Aguilera-Cortés LA, Martínez-Castillo J, Sauceda-Carvajal A, García-González L, Figueras-Costa E (2009a) A resonant magnetic field with high quality factor at atmospheric pressure. J Micromech Microeng 19:15016. doi:10.1088/0960-1317/19/1/015016

Herrera-May AL, Soto-Cruz BS, López-Huerta F, Aguilera-Cortés LA (2009b) Electromechanical analysis of a piezoresistive pressure microsensor for low-pressure biomedical applications. Rev Mex Fis 55:14–24

Hindrichsen CC, Almind NS, Brodersen SH, Hansen O, Thomsen EV (2009) Analytical model of a PZT thick-film triaxial accelerometer for optimum design. IEEE Sens J 9:419–429. doi:10.1109/JSEN.2009.2014412

Huang S, Li X, Song Z, Wang Y, Yang H, Che L, Jiao J (2005) A high-performance micromachined piezoresistive accelerometer with axially stressed tiny beams. J Micromech Microeng 15:993–1000. doi:10.1088/0960-1317/15/5/014

Kaltsas G, Goustouridis D, Nassiopoulou AG (2006) A thermal convective accelerometer system based on a silicon sensor-study and packaging. Sens Actuators A 132:147–153. doi:10.1016/j.sna.2006.04.026

Kovács A, Vízváry Z (2001) Structural parameter sensitivity analysis of cantilever-and bridge-type accelerometers. Sens Actuators A 89:197–205. doi:10.1016/S0924-4247(00)00553-7

Lee SJ, Cho DW (2004) Development of a micro-opto-mechanical accelerometer based on intensity modulation. Microsyst Technol 10:147–154. doi:10.1007/s00542-003-0324-9

Liu CH, Kenny TW (2001) A high-precision, wide-bandwidth micromachined tunneling accelerometer. J Microelectromech Syst 10:425–433. doi:10.1109/84.946800

Liu CH, Barzilai AM, Reynolds JK, Partridge A, Kenny TW, Grade JD, Rockstad HK (1998) Characterization of a high-sensitivity micromachined tunneling accelerometer with micro-g resolution. J Microelectromech Syst 7:235–244. doi:10.1109/84.679388

Llobera A, Seidemann V, Plaza JA, Cadarso VJ, Büttgenbach S (2007) SU-8 optical accelerometers. J Microelectromech Syst 16:111–121. doi:10.1109/JMEMS.2006.885845

Norton RL (2006) Machine design: an integrated approach, 3rd edn. Pearson Prentice Hall, New Jersey

Partridge A et al (2000) A high-performance planar piezoresistive accelerometer. J Microelectromech Syst 9:58–66. doi:10.1109/84.825778

Plaza JA, Collado A, Cabruja E, Steve J (2002) Piezoresistive accelerometers for MCM package. J Microelectromech Syst 11:794–801. doi:10.1109/JMEMS.2002.805213

Rao SS (2004) Mechanical Vibrations, 4th edn. Pearson Education Inc., Upper Saddle River

Roylance LM, Angell JB (1979) A batch-fabricated silicon accelerometer. IEEE Trans Electron Dev 26:1911–1917

Sankar AR, Lahiri SK, Das S (2009) Performance enhancement of a silicon MEMS piezoresistive single axis accelerometer with electroplated gold on a proof mass. J Micromech Microeng 19:025008. doi:10.1088/0960-1317/19/2/025008

Seidel H, Csepregi (1984) Design optimization for cantilever-type accelerometer. Sens Actuators 6:81–92

Senturia SD (2002) Microsystem design. Kluwer, Boston

Joshi BP, Chaware AS, Gangal SA (2005) Performance optimization of a cantilever-type micro-accelerometer. In: Proceedings of ISSS 2005, Bangalore, SB, pp 115–122

Yazdi N, Ayazi F, Najafi K (1998) Micromachined inertial sensors. In: Proceedings of the IEEE micro electro mechanical systems conference (MEMS'99), pp 1640–1659

Zhu M, Kirby P, Lim MY (2004) Lagrange's formalism for modeling of a triaxial microaccelerometer with piezoelectric thin-film sensing. IEEE Sens J 4:455–463. doi:10.1109/JSEN.2004.830948

Zou Q, Tan W, Kim ES, Loeb GE (2008) Single-and triaxis piezoelectric-bimorph accelerometers. J Microelectromech Syst 17:45–57. doi:10.1109/JMEMS.2007.909100